Free-electron-laser simulations: Effects of beam quality and space charge

J. Gardelle, J. Labrouche, and P. Le Taillandier
Commissariat à l'Energie Atomique, Centre d'Etudes Scientifiques et Techniques d'Aquitaine, BP2, 33114 Le Barp, France

Ph. Gouard
Commissariat à l'Energie Atomique, BP 27, 94190 Villeneuve-Saint-Georges, France
(Received 1 November 1993; revised manuscript received 1 August 1994)

In this paper we present numerical work we have done in electron beam transport and in free-electron-laser (FEL) simulation. We refer to the ONDINE1 experiment at Centre d'Etudes Scientifiques et Techniques d'Aquitaine, where we used a helical wiggler, a guiding magnetic field, and a low-energy high-current electron beam ($\approx$2 MeV, 1 kA). A brief description of the codes we have developed is given. Afterwards, we emphasize the effects of electron beam quality and space charge on FEL efficiency. The combined use of an electron beam transport code and a FEL code is a unique way to understand the difficulties encountered in such experiments, where the cathode was not immersed in the guiding field. Very good agreement has been found between experimental results and simulations.

PACS number(s): 41.60.Cr, 52.75.Ms, 41.85.Ja, 41.85.Lc

I. INTRODUCTION

Free-electron lasers (FEL) are now widely studied throughout the world as sources of coherent radiation over a broad spectrum from millimeter through optical wavelengths [1]. This paper concerns FELs which use a high-current ($\approx$1 kA) and low-energy ($\approx$1 MeV) electron beam. In such a case, a helical wiggler is often used to create the magnetic field that gives the basic periodic transverse motion which leads to radiation gain. Furthermore, a solenoid which produces a superimposed axial focusing magnetic field is necessary; the resulting magnetic field is a superposition of both. High peak power microwave radiation in the range 10–100 GHz has been produced in several laboratories [2]. The key to successful FEL operation is the electron beam quality. At present, accelerators for FELs are designed and built so as to reduce the emittance and the energy spread. Maintaining beam quality during electron beam propagation, on the one hand between the accelerator and the wiggler entrance, on the other hand inside the wiggler itself is certainly one of the most important problems in FEL operation.

A few years ago we ran a FEL experiment which failed [3]. The codes we used at that time were unable to explain the failure because they did not take into account the transport section with several solenoids we used in the experiment (i.e., they were not adapted to describe a nonimmersed FEL experiment). In fact, they only computed the FEL interaction with a constant guiding field. Since we needed a numerical tool to compute the characteristics of the electron beam at the beginning of FEL interaction (i.e., after its propagation through a magnetic line), we subsequently developed a beam transport code (the ELECTRA code). In this way, a realistic description of the electron beam at the wiggler entrance was obtained and used to provide input to FEL simulation by using the SOLITUDE code. The space-charge (SC) effects, which are often neglected at high energy, can become predominant at 1 MeV. Nonetheless, the assumptions we make to describe them prevent us from computing both transverse space-charge (TSC) and longitudinal space-charge (LSC) effects simultaneously. Thus their numerical effects on FEL interaction will be given separately.

The original idea in this work is the combined use of these two codes by taking into account the effects of SC to simulate a nonimmersed high-gain FEL experiment. We study in particular the characteristics of the electron beam just in front of the wiggler entrance where an axial magnetic field gradient may be present. The simultaneous use of these codes enables us to understand the principal causes of the erratic performance of the ONDINE 1 experiment.

The organization of the paper is as follows. A brief description of the first FEL experiment done at Centre d'Etudes Scientifiques et Techniques d'Aquitaine (CESTA) is given in Sec. II. General descriptions of ELECTRA and SOLITUDE are presented in Sec. III where we study in particular the effects of beam quality and SC. The combined use of the two codes to simulate the results of the ONDINE 1 FEL experiment is given in Sec. IV. Our conclusions are given in Sec. V.

II. DESCRIPTION OF THE ONDINE 1 EXPERIMENT

In the recent past, the Commissariat à l'Energie Atomique (CEA) had at CESTA a program to study high power FEL in the microwave frequency range using high brightness electron beams produced by induction linacs. Thermionic cathodes intended for use in the induction linac LELIA [4] were first studied with a pulse-line generator. With the electron beam generated, we seized the opportunity to run our first FEL experiment. However, the diode had been designed for hot cathode operation

and this precluded running in the immersed cathode configuration, which is generally used in the kind of experiment where the electrons are emitted in a constant axial guiding field.

After some work on the electron beam itself, we put a cold cathode in place of the thermionic one and ran the ONDINE 1 experiment. Its setup is illustrated in Fig. 1 and it was planned to operate either in superradiant or amplifier FEL regime at 35 GHz. It consisted of the pulse-line generator EUPHROSYNE, two focusing coils, and the pulsed helical wiggler and solenoid. The main parameters are listed in Table I.

Working in superradiance, a low FEL power (≈ 1 MW) was obtained with poor reproducibility. We suspected the cause was a significant beam quality degradation somewhere in the magnetic transport line.

III. GENERAL SIMULATION CODE RESULTS

We developed ELECTRA to compute the beam transport from the accelerator to the entrance of the wiggler. Then, SOLITUDE, which includes interaction with the rf electromagnetic field, calculates the electron trajectories and the rf power growth in the wiggler.

TABLE I. Main experimental parameters.

Electron beam parameters	
Current	$I=2700$ A
Energy	$T=2.2$ MeV
Pulse duration	$\tau=10$ ns, single shot
Beam radius	$r_e=5$–10 mm
Geometrical emittance	$\varepsilon\approx 1200\ \pi$ mm mrad
Position in z	$z=0$ m
Wiggler	
Type	Bifilar helix
Period	$\lambda_w=12$ cm
Length	$L_w=300$ cm
Number of adiabatic periods	$N_a=8$
Magnetic field on axis	$B_w<2000$ G
Position	$z=1.5$ m
Coil characteristics	
Coil no. 1	Position: $z_1=0.142$ m Length: $L_1=0.231$ m Magnetic field <1000 G
Coil no. 2	Position: $z_2=0.835$ m Length: $L_2=0.231$ m Magnetic field <1000 G
Coil no. 3	Position: $z_3=1.206$ m Length: $L_3=3.295$ m Magnetic field <10000 G
Best results	
Frequency	$f=35$ GHz
Power in K_a band (28–40 GHz)	1000 kW
Power at 35 GHz	200 kW

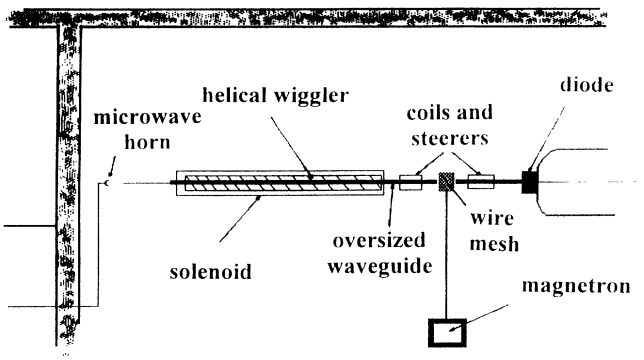

FIG. 1. The ONDINE 1 experimental configuration.

A. ELECTRA simulations

1. *Description of the code*

The first step in studying beam transport is generally to solve the envelope equation. It is a very simple and rapid way to obtain coil current adjustments in a magnetic transport line when beam energy, emittance, and current are known. In our case, more precise calculations were necessary and induced us to write the three dimensional (3D) stationary particle code ELECTRA which follows the electrons on their path in a magnet line and, in the case of interest here, from the cathode to the wiggler entrance.

Electron trajectories are computed by solving the equations of motion with a fifth-order Runge-Kutta method (the Merson method) [5]. A third-order magnetic field expansion is used to describe correctly off-axis motion. This is essential in our configuration because the electron beams delivered by pulsed diodes or induction linacs can have large transverse dimension (>1 cm): in some places, the radius of the electron beam may approach the radius of the transport coils. A beam transport line consisting of various components such as magnetic coils, steerers, accelerating gaps, wiggler magnet, and with different pipe radii or diaphragms can be studied in order to predict, for example, effects of coil misalignment on beam propagation.

Working at low energy (≈ 1 MeV), we particularly consider the effects of TSC fields. They are computed by solving the two following equations for the potentials:

$$\left[\frac{\partial^2}{\partial x^2}+\frac{\partial^2}{\partial y^2}\right]A_z(x,y)=-\frac{4\pi}{c}J_z(x,y)\ ,$$
$$\left[\frac{\partial^2}{\partial x^2}+\frac{\partial^2}{\partial y^2}\right]\Phi(x,y)=-4\pi\rho(x,y)\ , \tag{1}$$

with the assumption that the vector potential **A** has only a component in the z direction. Furthermore, the two potentials are assumed to be independent of z and time t. The solution is found by discretization on a 30×30 square mesh, depending only upon waveguide geometry. The error of discretization is insignificant if the transverse beam area corresponds to ten mesh intervals at least. Our assumptions exclude a LSC electric field E_Z.

However, in SOLITUDE, we have the possibility to include it as described later.

2. *Simulation of the ONDINE 1 transport*

When we study the ONDINE 1 experiment, the ELECTRA initial conditions are provided by measurements of the beam parameters at the diode exit just behind the anode. First, they are used to run the envelope code. Figure 2 shows the beam radius obtained with the settings of the two associated coils. The ELECTRA results shown in Fig. 3 are very similar. In this example we have plotted the radii of several electron trajectories as functions of z, the axis of propagation. Betatron oscillations appear for $z > 1.2$ m and are visible in both codes. They are caused by electron beam mismatch at the solenoid entrance. A slightly different magnetic field adjustment would have given an electron beam radius close to the equilibrium radius corresponding to a cylindrical envelope. During experiments, we measured a beam loss of roughly 30% at the exit of the first guiding coil just as we obtain in the simulation where some particles hit the 3 cm radius pipe at this position (see Fig. 3).

Our computation stops at the wiggler entrance where the axial guiding field B_0 added to the wiggler field becomes constant. We use these results as initial conditions in the SOLITUDE code. Inspection of the beam structure at this position ($z = 1.5$ m) reveals a very important axial energy spread due to cyclotronic motion generated by the axial magnetic field gradient at the solenoid entrance [Fig. 4(a)]. This effect, when associated with TSC, also leads to a significant total energy spread as we can see in Fig. 4(b). The corresponding trace phase X'-X is shown in Fig. 4(c). The area occupied corresponds to a so-called effective geometrical emittance of 2800 π mm mrad. It is eight times greater than the original value of 350 π mm mrad. This enhancement comes from an azimuthal velocity dispersion which occurs during the beam's entrance into the solenoid. There, the gradient in B_0 induces a radial field B_r which depends on the radial position r. It produces a dispersion of the cyclotronic motion and increases the volume occupied in the trace phase.

B. The SOLITUDE code

With the 1D FEL linear theory one can obtain operational parameters and estimations of efficiency or saturation length in both the high-gain Compton and Raman regimes [6]. Knowledge of the energy, current, and electron beam radius permits one to solve the 1D linear dispersion equation. Then, for each pair of magnetic fields (B_0, B_w) corresponding to stable orbits, the interaction frequency and corresponding linear growth rate can be calculated. Here B_0 denotes the axial guiding field and B_w is the wiggler field amplitude. The subsequent gyroresonance, where the cyclotron period in the guiding field B_0 approaches the wiggler period, is the dividing line between the so-called group I and group II regions of operation. This occurs at [6]

$$\Omega_0 = \gamma k_w v_z \ , \tag{2}$$

where $\Omega_0 = eB_0/m$ is the nonrelativistic cyclotron frequency, $\gamma = [1-(v^2/c^2)]^{-1/2}$ is the relativistic factor, $k_w = 2\pi/\lambda_w$ is the wiggler wave number, and v_z is the electronic axial velocity. It is very difficult to work near this region because transverse velocities are very large and the electron beam can be lost by striking the wall of the pipe. For our parameters, the best amplification was expected in group II (high guiding field region) with a compromise between the high gain obtained near the resonance and the loss of electrons due to unstable orbits. It has been recently demonstrated that another regime exists which uses negative values of guiding field obtained by reversing its direction. One of the maximum experimental FEL efficiencies has been measured in this reversed field regime [7].

Although it is possible to improve 1D theory with 3D corrections [8], it is necessary to use 3D nonlinear simulation codes to compute efficiency or to study saturation by taking into account an actual electron beam. Its initial parameters can be obtained either by measurements or by computation done with a reliable electron transport code such as ELECTRA. Knowledge of these initial conditions is essential.

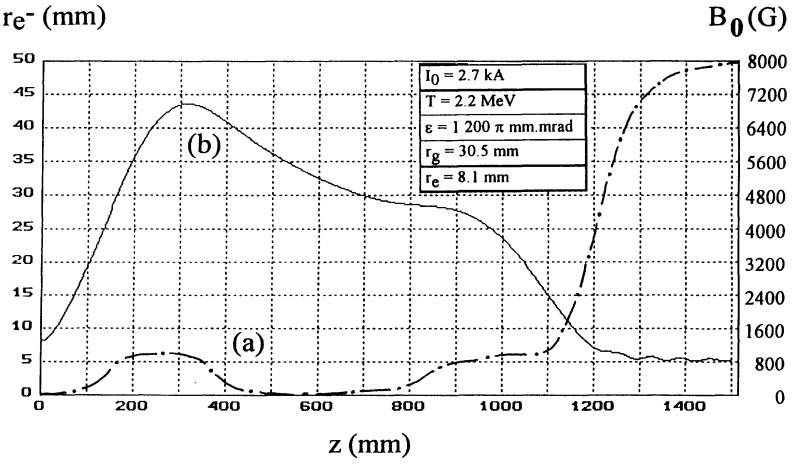

FIG. 2. Right hand scale: (a) typical magnetic field profile in the ONDINE 1 transport region (two coils and a solenoid) as calculated by the envelope code. Left hand scale: (b) radius of the electron beam envelope predicted by the envelope equation.

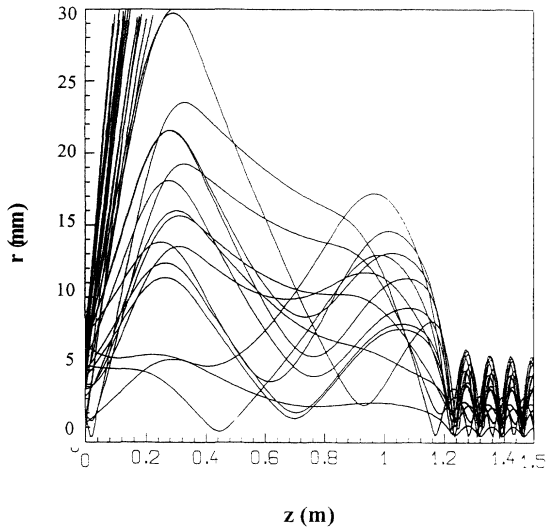

FIG. 3. Electron radial position vs z for 40 sample electrons as computed with ELECTRA. One can see current loss occurring in the first guiding coil for $z \approx 20$ cm. In this example, betatron oscillations seen on the right could be minimized by a better choice of coil currents.

1. *Description of SOLITUDE*

The SOLITUDE code is a single-frequency, nonlinear 3D simulation code designed for the purpose of studying FEL amplifier experiments [9]. The electromagnetic wave to be amplified propagates in a cylindrical waveguide and is developed in TE and TM modes. With the SVAP (slowly varying amplitude and phase) approximation [10], we can solve Maxwell's equations by averaging over a wave period λ and obtain the amplitude and phase evolution of the fundamental TE_{11} mode. Coupling of higher modes is not yet included in SOLITUDE whereas they can be investigated with the ARACHNEE code [11]. In fact, SOLITUDE uses the same FEL formalism as ARACHNEE, with a slightly different numerical method, but with significant differences in the description of the electron beam and in the computation of the space-charge effects.

Electron trajectories are computed by integrating the Lorentz force equation. The wiggler field is linearly increased from zero to its nominal value in the adiabatic entrance consisting of N_a wiggler periods. The coupled system of nonlinear differential equations obtained is solved by using the variable step Merson method mentioned above.

We can take into account TSC by solving Eqs. (1) as we do in ELECTRA to obtain the self-fields E_x, E_y and B_x, B_y. This calculation is different from the one recently added to ARACHNEE [12] where an idealized model permits one to obtain analytical expressions for the self-fields. Its hypothesis consists in considering the electron beam fixed along the z axis and is too restrictive for us.

Since the potential Φ does not depend on z, one cannot compute the electrical field E_z at the same time. Hence the effects of LSC that can be important in a FEL work-

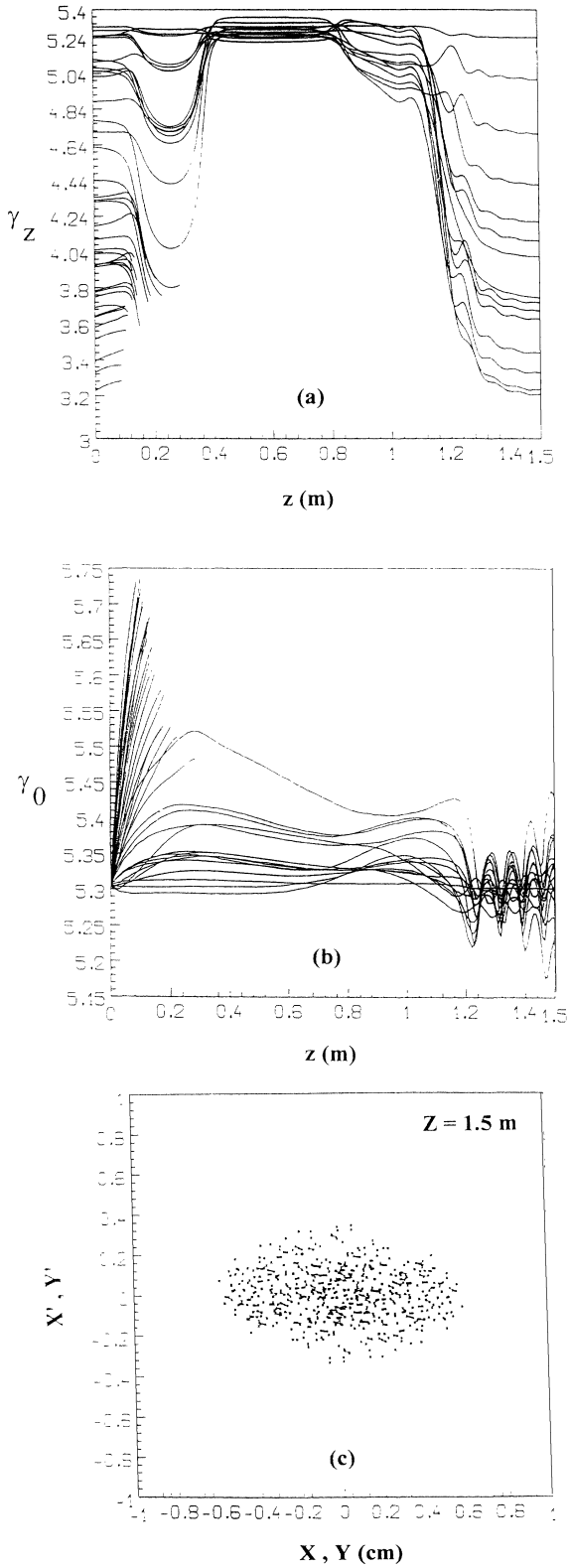

FIG. 4. Electron beam quality showing (a) axial energy vs z with a very large axial energy dispersion due to cyclotron motion in the solenoid fringing field; (b) total energy vs z with a spread coming from space charge (roughly 4%); and (c) corresponding phase spaces (X',X) and (Y',Y) at the wiggler entrance ($z = 1.5$ m), showing a large effective emittance enhancement (from 350 to 2800 π mm mrad in this case).

ing in the Raman regime can only be studied by neglecting TSC. The same hypothesis that is used in the ARACHNEE code has been used [11] to incorporate LSC into SOLITUDE.

2. *General results from SOLITUDE*

Figure 5 gives SOLITUDE predictions for the NRL Ubitron experiment [13]. They agree very well with the curves computed by ARACHNEE, both in the Compton FEL regime where LSC effects are neglected (circles) and in the Raman FEL regime where it is taken into account (triangles). We show by using SOLITUDE that including TSC in the Compton case does not change the results (squares).

The earliest studies with the ONDINE 1 parameters were done assuming a perfect electron beam (monoenergetic, zero emittance, and on-axis injection) and without SC effects. As we said before, the linear theory provides a set of optimized magnetic field pairs (B_0, B_w) in both group I and II: Table II shows some of them for 2.5 MeV, $I=1$ kA, and $r_{e\_}=5$ mm. The maximum power in the TE_{11} mode computed with SOLITUDE is obtained for values which are very close to the theoretical B_0 value predicted by the linear theory. This is indicated in Table II where we have chosen to fix the value of B_w obtained by the linear theory and we have made a sweep in B_0. Power in the TE_{11} mode versus the distance z, phase space (γ, ψ) at a given z, and one-electron tracking over z are typical outputs from SOLITUDE. Examples are given in Fig. 6 for the (8000,1000) group II reference pair which yields the maximum efficiency (35%). In this case, we assumed a perfect homogeneous beam. The curve giving power versus z shows that saturation is reached at $z=3.8$ m [Fig. 6(a)]. The phase-space plot exhibits the well-known bucket shape at $z=3.5$ m, just before saturation [Fig. 6(b)]. The high electromagnetic power can strongly perturb the electronic motion. This effect is evident in the sample trajectory seen in Fig. 6(c) at this location. Figure 7 represents a close-up in a (B_0, B_w) plane around a high peak power pair (500 MW) showing the bandwidth in magnetic fields, arbitrarily defined for an amplification greater than 1 MW:

$$\Delta B_0 \approx 550 \text{ G}, \quad \Delta B_w \approx 150 \text{ G} .$$

These results are important for choosing the step in magnetic fields when running single shot experiments.

TABLE II. Examples of 35 GHz resonant magnetic field pairs. Kinetic energy: $T=2.5$ MeV; beam current: $I=1$ kA; beam radius: $r_e=5$ mm. In parentheses are given the values of B_0 maximizing the 1D linear growth rate. It is very close to the value found by SOLITUDE which gives the maximum power.

B_0 (G)	B_w (G)	P_{TE11} (MW)
	Group I	
3950	250	196
2950	500	256
(2800)		
2000	750	426
1000	1050	488
	Group II	
5850	250	507
(5750)		
6550	500	260
(6700)		
7350	750	383
(7460)		
8050	1000	982
(8200)		
8900	1250	624
(9060)		
10200	1500	210
(9980)		

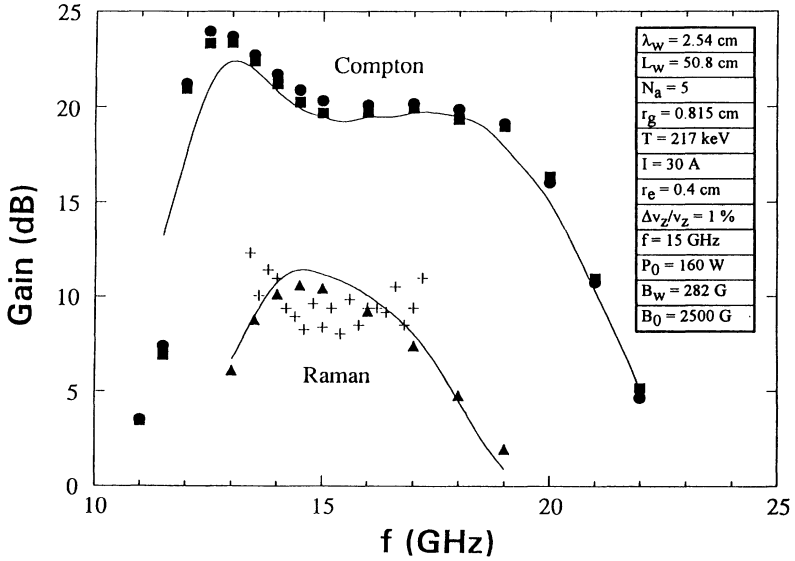

FIG. 5. Comparison between SOLITUDE and ARACHNEE for the NRL Ubitron. The curves show gain as a function of frequency. Circles are simulations which neglect the effects of SC, squares are results obtained with TSC effects, and both are quite similar. The Raman case obtained by including LSC effects is shown by triangles which are in very good agreement with crosses representing experimental results. The solid lines represent ARACHNEE results.

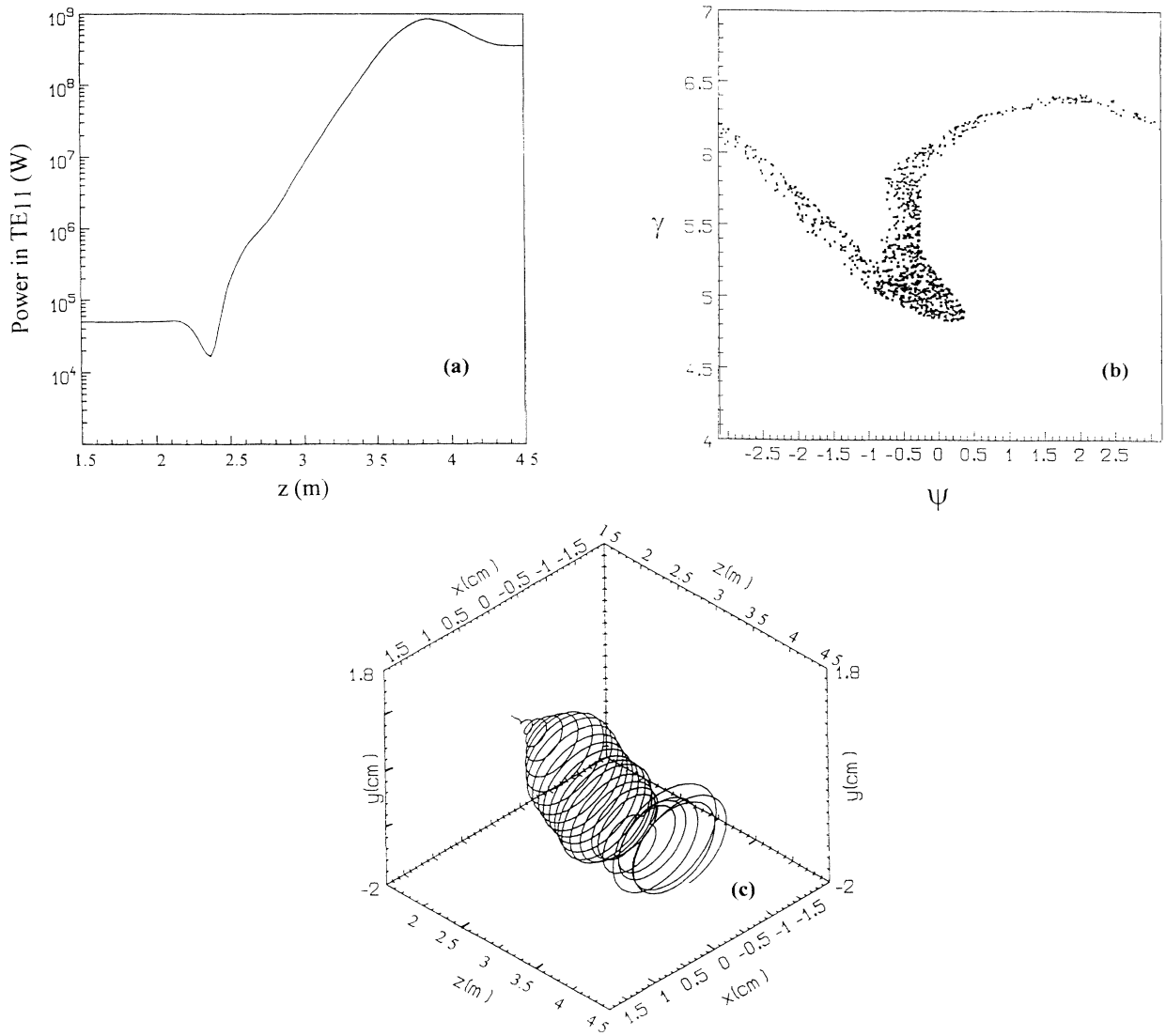

FIG. 6. Example of ONDINE 1 simulation for the (8000,1000) group II pair (with zero emittance and zero energy spread). (a) TE_{11} power vs z, (b) phase-space plot at $z = 3.5$ m just before saturation, (c) typical electron orbit along the 3 m interaction length.

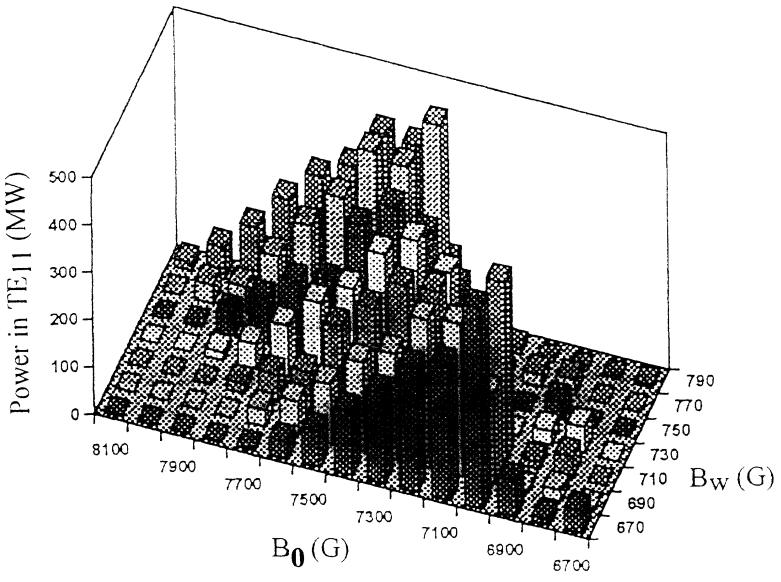

FIG. 7. A close-up in the (B_z, B_w) plane around a high efficiency pair (B_0, B_w) shows the magnetic field ranges corresponding to power ≥ 1 MW: 300 G in B_w and 1000 G in B_z around the 500 MW pair (7500,750).

3. *Effects of space charge on performance*

Special attention has been paid to TSC and LSC effects. They are given here for the reference pair in group II (8000,1000) [Fig. 8(a)] and for another pair at low guiding field (2000,750) in group I [Fig. 8(b)]. As we can see, if SC is present great care is required when drawing conclusions because maxima in power are shifted due to changes in the axial velocity. So, we need to make a sweep in one of the magnetic fields, B_0, for example. In group I, we do not see a decrease in power but only this shift. In contrast, for group II, TSC effects are much more important and lead to a 20% reduction in power. This reduction would increase with introduction of beam emittance. Then, we conclude that in experiments similar to the Ubitron experiment, but working at higher energies, TSC can play an important role.

4. *Effects of beam quality*

FEL operating parameters can be obtained more rapidly with ARACHNEE, but we believe a more accurate and physical description of the electron beam, especially in our configuration with several correcting coils, can be obtained with SOLITUDE. For example, we can look at power reduction due to emittance, misalignment, and off-center wiggler injection: all these effects reduce efficiency (see Table III). The electronic distribution used here is Gaussian in transverse position; the beam is assumed to be monoenergetic whereas the transverse velocities are obtained from an ellipse of emittance. This latter is described by using Twiss parameters [14]. In the example presented the ellipse is degenerate; it corresponds to a beam waist. In Table III, for the zero emittance runs, we can see that a misalignment increases power for the (8000,1000) reference pair. A misalignment is analogous to a beam slope at wiggler injection with a value of the axial velocity v_z which is smaller and closer to the ideal value for the best interaction with the rf field at 35 GHz. Decreasing v_z can also be done by decreasing B_0: the pair (8050,1000), which gives the maximum power in the perfect beam case (Table II), gives the correct value of v_z.

It appears more reasonable to predict the effects of beam quality on FEL efficiency using readily accessible experimental parameters such as emittance rather than using an effective energy spread $\Delta\gamma_z/\gamma_z$ which is not easily measured. Although expressions can be found to connect this latter quantity with emittance or space charge [15], the approximations made are quite restrictive for the low-energy and high-current beams which concern us. In our opinion, using an effective axial energy spread as a free parameter to fit experimental data is

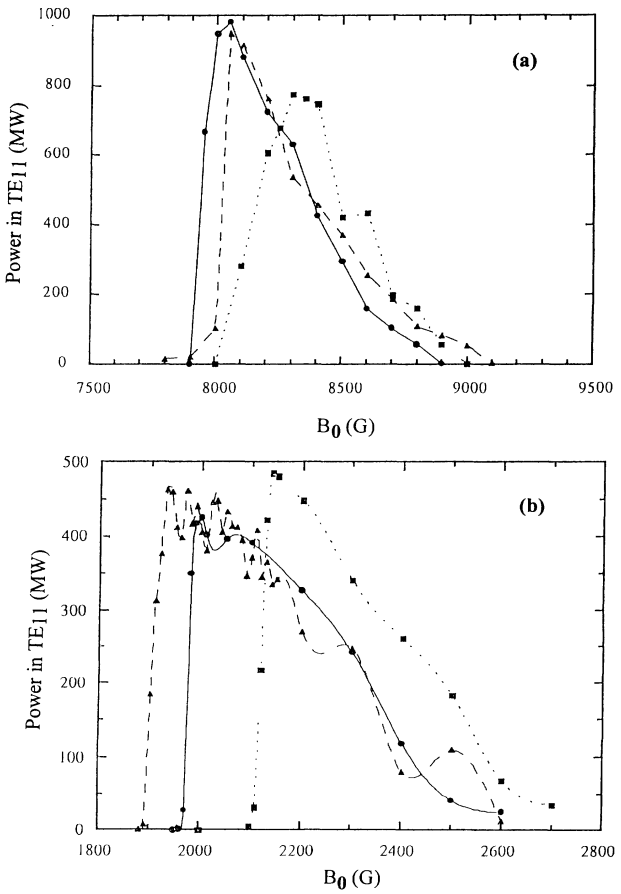

FIG. 8. Illustration of space-charge (SC) effects with a "perfect beam." Circles are computed neglecting SC, squares correspond to including TSC, and triangles to taking into account LSC. TSC effects are more important than LSC effects: (a) power vs B_0 in group II; (b) power vs B_0 in group I.

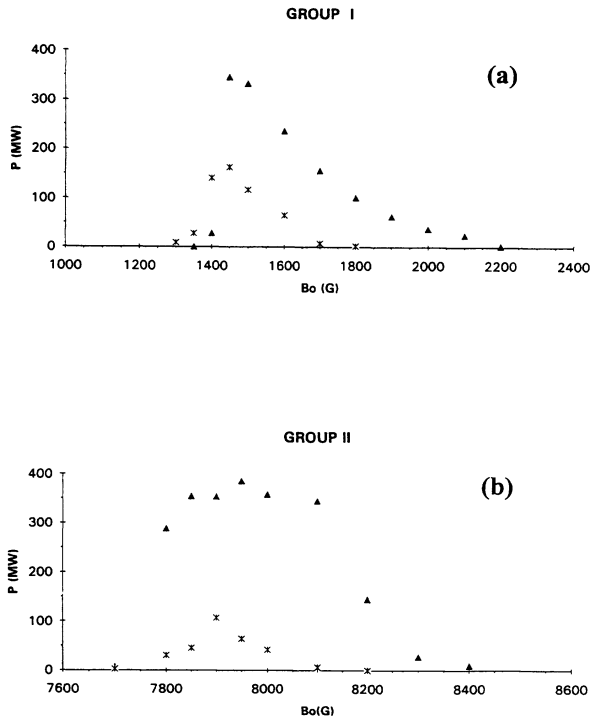

FIG. 9. Power vs B_0 including TSC effects. Crosses are results obtained from the combined use of ELECTRA and SOLITUDE whereas black triangles correspond to SOLITUDE predictions made using an ideal beam. Substantial power loss is observed, especially in group II. The beam kinetic energy is 2.2 MeV: (a) group I, $B_w = 750$ G; (b) group II, $B_w = 1000$ G.

TABLE III. Effects of beam emittance, decentering, and misalignment on beam power for two pairs (B_0, B_w) in groups I and II; $T=2.5$ MeV, $I=1$ kA, $r_e=5$ mm.

Emittance ε (π mm mrad)	Decentering r_0 (cm)	Misalignment α (deg)	P (MW) (8200,1000) group II	P (MW) (3950,250) group I
0		0	643	160
	0	2	709	144
		4	724	149
		0	544	135
	0.5	2	525	156
		4	454	105
		0	204	4
	1	2	212	1
		4	204	2
500		0	613	58
	0	2	521	12
		4	392	7
		0	416	57
	0.5	2	391	25
		4	315	9
		0	2	
	1	2	5	
		4	1	

not a very profitable exercise. It is more useful to calculate tolerances based on experimentally observable beam parameters such as alignment or emittance.

IV. COMBINED USE OF SOLITUDE AND ELECTRA

In order to simulate the effects of beam quality and SC on the ONDINE 1 experiment, we have coupled the two codes described above. The initial positions, velocities, and energies of each electron at the SOLITUDE input are furnished by the ELECTRA output. The following calculations are made now at 2.2 MeV, which corresponds to the ONDINE 1 experimental energy. As before we investigate two cases, one in each FEL group. Figure 9 shows power in the TE_{11} mode as a function of B_0. Black triangles correspond to SOLITUDE runs, including TSC, assuming a perfect electron beam but using the electron beam radius and current given by ELECTRA at the wiggler entrance. Electrons are monoenergetic with zero transverse momentum and one finds the maximum efficiency. The power is lower than results shown in Fig. 8 because beam radius is greater in this case. Therefore the electronic current density is lower, leading to less efficiency. Crosses correspond to runs obtained by coupling ELECTRA and SOLITUDE with TSC. These results clearly show the effects of beam quality, which leads in both groups to a narrowing of the bandwidth defined previously (Sec. III B 2). This narrowing is very drastic in group II where we lose the large band in B_0 leading to a high power we have obtained assuming a perfect beam (black triangles in the curve). The power levels reached must be considered separately in group I and group II. For group I [Fig. 9(a)], we lose half the power but for group II [Fig. 9(b)], roughly 75% is lost. As we showed before, the effective emittance is enhanced by the solenoid gradient. Working in group I means that B_z and its associated gradient are not very high. The power reduction is consequently less than expected in group II, where the gradient is much more important.

Although SOLITUDE is an amplifier code we can nevertheless compare this power reduction with the typical 1 MW power level obtained experimentally in the superradiant case instead of the 5 to 10 MW which were expected on the basis of efficiency obtained in similar immersed cathode FEL experiments.

V. CONCLUSIONS

We have investigated free-electron lasers with a helical wiggler but where the guiding field is not constant along the axis of propagation. This corresponds to a transport section from the cathode to the wiggler entrance. We have written the ELECTRA code to examine beam transport while we have developed the SOLITUDE code to compute FEL amplification. We have focused on the effects of space charge and electron beam quality.

Results obtained from SOLITUDE only, for the parameters of the experiment described, showed that transverse space charge can play an important role in group II by shifting the resonance and decreasing the efficiency. Introduction of a realistic beam emittance (corresponding to measurements at the diode output) was not enough to explain the low power levels observed in the experiment. In fact, we have understood the failure of the ONDINE 1 experiment by combining the FEL code with ELECTRA. A strong magnetic field gradient appears before the wiggler entrance when working in group II (high guiding solenoidal field). It causes an efficiency degradation by increasing the transverse motion in such a way that the

effective emittance at the wiggler entrance becomes very large. In fact, from the results of this numerical work we can understand quantitatively why in a non-immersed cathode FEL experiment using a helical wiggler and high axial guiding magnetic field and working with low-energy, high-current, and high emittance beams, one cannot reach high power levels. Furthermore, the greater the initial emittance, the more significant the gradient effect will be. This kind of FEL is really efficient only when working in an immersed configuration.

[1] T. C. Marshall, *Free Electron Lasers* (Macmillan, New York, 1985); P. Luchini and H. Motz, *Undulators and Free Electron Lasers* (Clarendon, Oxford, 1990); H. P. Freund, and T. M. Antonsen, Jr., *Principles of Free Electron Lasers* (Chapman and Hall, London, 1992).

[2] S. H. Gold, W. M. Black, H. P. Freund, V. L. Granatstein, and A. K. Kinkead, Phys. Fluids **27**, 746 (1984); J. Fajans, J. S. Wurtele, G. Bekefi, D. S. Knowless, and K. Xu, Phys. Rev. Lett. **57**, 579 (1986); F. G. Yee, T. C. Marshall, and S. P. Schlesinger, IEEE Trans. Plasma Sci. **PS-16**, 162 (1988); K. L. Flech, L. Vallier, J. M. Buzzi, P. Drossart, H. Boehmer, H. J. Doucet, B. Etlicher, H. Lamain, and C. Roullié, IEEE J. Quantum Electron. **QE-17**, 1354 (1981).

[3] H. Bottollier-Curtet, J. Gardelle, J. Bardy, C. Bonnafond, A. Devin, G. Germain, J. Labrouche, J. Launspach, P. Le Taillandier, and J. de Mascureau, Nucl. Instrum. Methods Phys. Res. Sect. A **304**, 197 (1991).

[4] J. Launspach, J. M. Angles, M. Angles, P. Anthouard, J. Bardy, C. Bonnafond, H. Bottollier-Curtet, A. Devin, Ph. Eyharts, P. Eyl, J. Gardelle, G. Germain, P. Grua, J. Labrouche, J. de Mascureau, P. Le Taillandier, W. Stadnikoff, and M. Thevenot, Nucl. Instrum. Methods Phys. Res. Sect. A **304**, 368 (1991).

[5] A. Ralston and H. S. Wilf, *Méthodes Mathématiques pour Calculateurs Arithmétique* (Dunod, Paris, 1965), p. 155.

[6] H. P. Freund, P. Sprangle, D. Dillenburg, E. H. da Jornada, R. S. Schneider, and B. Liberman, Phys. Rev. A **26**, 2004 (1982).

[7] M. E. Conde and G. Bekefi, Phys. Rev. Lett. **67**, 3082 (1981).

[8] H. P. Freund, S. Johnston, and P. Sprangle, IEEE J. Quantum Electron. **QE-19**, 3 (1983) **QE-19**, 322 (1983); H. P. Freund and A. K. Ganguly, *ibid.* **QE-21**, 7 (1985); **QE-21**, 1073 (1985).

[9] Ph. Gouard and J. Gardelle, Commissariat à l'Energie Atomique Report No. CEA-R-5617, 1992 (unpublished).

[10] W. B. Colson, IEEE J. Quantum Electron. **QE-17**, 1417 (1981); N. M. Kroll, P. L. Morton, and M. N. Rosenbluth, *ibid.* **QE-17**, 1436 (1981).

[11] A. K. Ganguly and H. P. Freund, Phys. Fluids **31**, 2 (1988); **31**, 387 (1988); A. K. Ganguly and H. P. Freund, Phys. Rev. A **32**, 2275 (1985).

[12] H. P. Freund, R. H. Jackson, and D. E. Pershing, Phys. Fluids B **5**, 2318 (1993).

[13] D. E. Pershing, R. H. Jackson, H. P. Freund, and H. Bluem, Nucl. Instrum. Methods Phys. Res. Sect. A **285**, 56 (1989).

[14] J. D. Lawson, *Physics of Charged Particle Beams,* 2nd ed. (Clarendon, Oxford 1988), p. 165.

[15] C. W. Roberson, J. A. Pasour, F. Mako, R. F. Lucey, Jr., and P. Sprangle, in *Infrared and Millimeter Waves,* edited by K. J. Bulton (Academic, New York, 1983), Vol. 10, pp. 361–398.

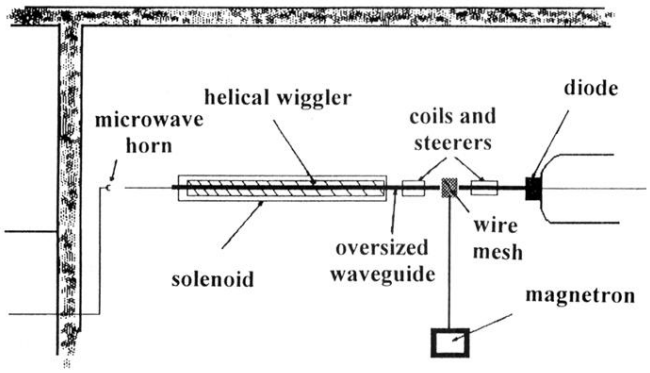

FIG. 1. The ONDINE 1 experimental configuration.

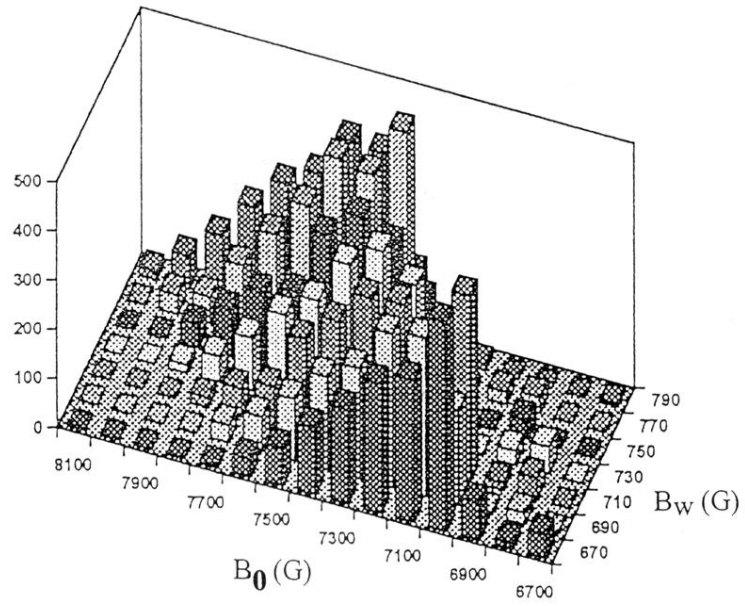

FIG. 7. A close-up in the (B_z, B_w) plane around a high efficiency pair (B_0, B_w) shows the magnetic field ranges corresponding to power ≥ 1 MW: 300 G in B_w and 1000 G in B_z around the 500 MW pair (7500,750).